



RESEARCH LETTER

10.1002/2015GL064917

Key Points:

- Resonant frequencies of a natural arch deduced from ambient seismic data
- Numerical modal analysis used to clarify resonant mode shapes
- Diurnal frequency shifts ascribed to thermal stresses

Supporting Information:

- Figures S1–S5, Movie S1 caption, Data Set S1 description, and Text S1
- Movie S1
- Data Set S1

Correspondence to:

J. R. Moore,
jeff.moore@utah.edu

Citation:

Starr, A. M., J. R. Moore, and M. S. Thorne (2015), Ambient resonance of Mesa Arch, Canyonlands National Park, Utah, *Geophys. Res. Lett.*, 42, doi:10.1002/2015GL064917.

Received 11 JUN 2015

Accepted 24 JUL 2015

Accepted article online 5 AUG 2015

Ambient resonance of Mesa Arch, Canyonlands National Park, Utah

Alison M. Starr¹, Jeffrey R. Moore¹, and Michael S. Thorne¹

¹Department of Geology and Geophysics, University of Utah, Salt Lake City, Utah, USA

Abstract We analyzed the resonance characteristics of a prominent natural arch in Canyonlands National Park, Mesa Arch, as measured from ambient seismic data. Evaluating spectral and polarization attributes, we distinguished the first four resonant frequencies of the arch, 2.9, 6.0, 6.9, and 8.5 Hz, as well as basic properties of the associated mode shapes. We then affirmed experimental data using 3-D numerical modal analysis, providing estimates of material properties and clarifying vibrational mode shapes. Monitoring resonant frequencies over time, we searched for shifts associated with changing environmental conditions and long-term progressive damage. We measured ~3% direct daily variation in resonant frequency associated with changing rock temperature, thermal stress, and stiffening of the rock matrix. Independent tilt data showed similar diurnal cycles associated with thermoelastic stresses and deformation of the arch. We observed no permanent resonant frequency shifts related to irreversible damage of Mesa Arch during our study period.

1. Introduction

Rock arches are dynamic natural structures that vibrate with measurable resonant frequencies and mode shapes. Vibration characteristics are in turn tied to fundamental material properties, density, and elastic modulus, making ambient vibration monitoring a powerful, noninvasive tool for assessment of changing structural integrity. However, the resonance properties of natural arches have not been previously studied in detail, despite the prevalent use of related structural health monitoring (SHM) techniques in civil engineering [e.g., *Carder*, 1936; *Crawford and Ward*, 1964; *Sohn et al.*, 1999]. Central to the idea of SHM is that a change in the deformability of mechanical elements within a system leads to a change in the global vibrational response [*Farrar et al.*, 2001]. Measurements of vibration characteristics over time may thus provide evidence of internal mechanical change, while short- and long-term monitoring can differentiate reversible versus irreversible signals [*Clinton et al.*, 2006].

Application of SHM techniques to natural rock structures is an emerging method in surface processes research. *Lévy et al.* [2010], for example, showed that the fundamental frequency of an unstable rock column dropped by 24% prior to collapse. They posited that a growing fracture separating the column increased the volume of the body, decreasing the resonant frequency. Superposed reversible fluctuations were attributed to thermal and hydrological effects. *Bottelin et al.* [2013a, 2013b] analyzed thermal and spectral data at a similar rock column, monitoring daily and seasonal changes in resonant frequency. Frequency shifts were related to thermal expansion and winter ice stiffening the connection between the column and cliff. Meanwhile, *Burjanek et al.* [2010, 2012] and *Moore et al.* [2011] used ambient vibration measurements to identify anisotropy, wavefield polarization, and spectral amplification within large unstable rock masses, results with implications for seismic slope stability.

We document the resonant frequencies and mode shapes of a prominent rock arch in Canyonlands National Park, Utah, as measured from ambient seismic data. We identify reversible changes in resonant frequencies associated with environmental effects, search for signals of irreversible change linked to internal damage, and ultimately aim to develop new methodology for quantitative evaluation of the changing structural health of natural rock arches.

2. Study Site

Mesa Arch is one of the premier attractions of Canyonlands National Park, Utah (Figure 1). The arch measures ~2.5 m thick and ~3 m wide and spans 27 m at the edge of a plateau. On close inspection, Mesa Arch is seen to be part of a large vertical slab of Navajo sandstone partly detached from the plateau edge (Figure 1b). A crack

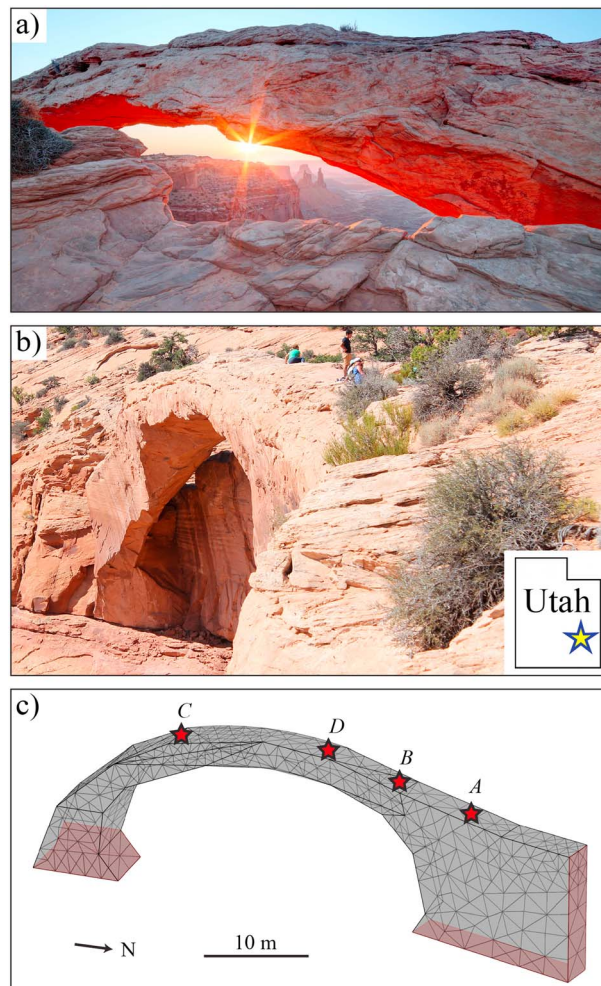


Figure 1. Mesa Arch: (a) scenic sunrise view (image: C. Dorsey), (b) view to the south showing southern abutment and base (inset: location), and (c) 3-D model and finite-element mesh. Seismometer positions A–D used for resonance measurements. External boundaries shaded red are fixed in modal analysis.

to investigate seasonal effects and search for long-term frequency shifts. On the daily scale, we monitored resonant frequencies continuously over a 3 day period in May 2014, with the goal of identifying daily frequency shifts and associated drivers. As Mesa Arch is a high-profile feature of Canyonlands National Park, longer-duration continuous monitoring was not possible. We reoccupied the same primary measurement location in most experiments; the position (labeled A in Figure 1c) is located on the northern end of the arch and allows safe access in all seasons. Additional experiments designed to measure resonant mode shapes and polarization attributes occupied different sensor positions (B–D in Figure 1c).

Ambient vibration measurements were typically conducted in a site-to-reference configuration using two seismometers: one placed on the arch (termed active sensor) and the other placed on flat bedrock roughly 90 m away for reference (Figure S2). This allowed us to isolate signals of interest related to resonance of the arch. We used Nanometrics Trillium-Compact broadband seismometers (flat frequency response between 0.05 and 100 Hz) with 24 bit Centaur data loggers. Ambient vibration data were recorded at 100 Hz. We monitored deformation of Mesa Arch during our 3 day experiment using a Jewell Instruments 701-2(4X) biaxial tilt meter. The instrument was placed on top of the arch roughly 1 m from seismometer position A; tilt data were temperature corrected. We simultaneously monitored rock surface temperature, as well as air temperature and relative humidity, using Onset Hobo U23 data loggers (Figure S1b).

running >10 m horizontal length and ~ 10 m depth delineates the northern abutment (Figure S1a in the supporting information). Farther north, this crack fills with sand and merges into intact bedrock. On its southern end, Mesa Arch stands freely as the abutment dives steeply into the cliff. A basal discontinuity separates the arch and slab from the cliff below. Mesa Arch trends roughly north-south with a slight curve (Figure S2).

Past arch collapses in the Moab, Utah, area underscore the relevance of investigating new methods to understand damage mechanics. In August 2008, Wall Arch in Arches National Park collapsed unexpectedly along a popular trail. Images of the arch before collapse showed a thick but sagging span. Meanwhile Landscape Arch, located along the same trail, is North America's longest arch; slab failures in 1991 and 1995 resulted in closure of a trail under the arch. In the greater Moab area, Courthouse Arch collapsed in 1988/1989, Cave Arch fell in 1995/1996, while Arrowhead Arch collapsed in 2010, among others.

3. Experiments

We conducted experiments at Mesa Arch on two timescales: daily and seasonal. We measured ambient resonance every 2 months between September 2013 and October 2014, and again in May 2015,

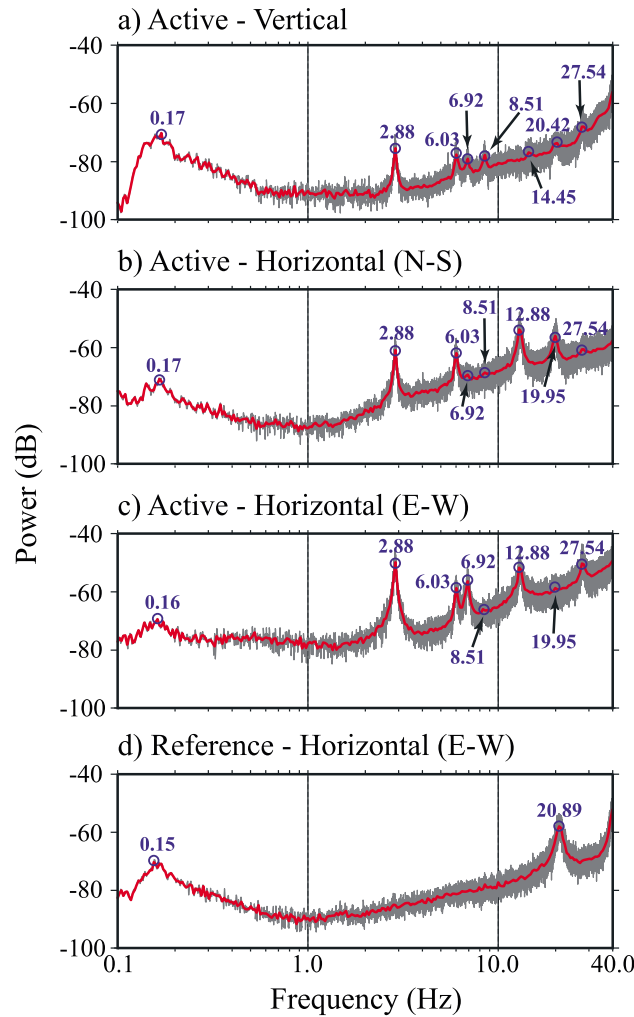


Figure 2. Power spectral density (PSD) from 28 September 2013 measurement. (a–c) PSD for three components of active sensor data on Mesa Arch (position A) and (d) east-west horizontal component of the reference sensor. Primary spectral peaks are circled and labeled.

Ambient vibration data were processed for spectral content, polarization magnitude, and orientation. We first removed the mean and trend from each trace. Next we removed the instrument response by spectral division, and band-pass filtered data between 0.002 and 50 Hz. We then computed the power spectral density (PSD) by fast Fourier transform and averaged the PSD in equally spaced bins in log10 space [McNamara and Buland, 2004; Sufri et al., 2014]. For polarization analysis, we used an adaptation of the technique described by Park et al. [1987], which measures polarization at distinct frequencies [Koper and Hawley, 2010] (see supporting information). We calculated the dominant horizontal azimuth and incidence angle (dip) of particle motion, the degree of polarization, and phase rotation between horizontal-to-horizontal components and horizontal-to-vertical components.

4. Modal Analysis

Ambient vibration data from Mesa Arch revealed several distinct spectral peaks at frequencies between ~3 and 9 Hz, each of which was not present on the reference sensor (Figure 2). These we interpret as resonant frequencies of the arch and explore through experimental and numerical modal analysis.

4.1. Experimental

The first four resonant frequencies of Mesa Arch are approximately 2.9, 6.0, 6.9, and 8.5 Hz (Figure 2 and Table 1). Each spectral peak was identified in repeat ambient vibration measurements over ~1.5 years (Table 2). For simplicity, we show in Figure 2 data collected on 28 September 2013 from sensor position A but discuss overall spectra and polarization results from all data sets.

We interpret the first spectral peak (f_1) at 2.9 Hz as the fundamental frequency of vibration of Mesa Arch (Figure 2); power is strongest on the E-W horizontal component at ~30 dB above background. Ground motion is strongly polarized (degree of polarization = 1.0 representing linear motion) and oriented at azimuth of 099°–108°, perpendicular to the trend of the arch, with horizontal incidence angles (86°–89°). The second spectral peak (f_2) at 6.0 Hz represents again primarily horizontal motion, with dominant azimuth of 111°–142° and incidence angles around 85°. Polarization magnitude is ~0.9. The third spectral peak (f_3) at 6.9 Hz has dominant azimuth of 83°–101° and incidence angles between 85° and 90°; the degree of polarization is ~0.9. Peak f_4 at 8.5 Hz is strongest on the vertical component. Dominant azimuth is 029°–067° with incidence angles 65–80°; the degree of polarization is ~0.6 (Table 1).

Spectral peaks >10 Hz occur regularly in our data, e.g., at ~13 and ~27 Hz (Figure 2). However, these are less consistent between measurements than the four resonant frequencies described above and are therefore

Table 1. Measured Frequencies and Polarization Attributes for the First Four Resonant Modes of Mesa Arch, Shown Together With Modeled Values; Sensor Position A (Figure 1c)

Mode	Frequency (Hz)	Degree of Polarization (0–1)	Azimuth ^a (deg)	Incidence ^b (deg)	Modeled Frequency (Hz)	Modeled Azimuth (deg)/Incidence (deg)
1	2.9–3.1	1.0	099–108	86–89	3.0	102/89
2	5.9–6.6	0.8–1.0	111–142	83–86	6.0	106/90
3	6.9–7.6	0.8–1.0	083–101	85–90	7.1	034/59
4	8.2–8.8	0.5–0.7	029–067	65–83	8.1	058/80

^aDegrees from magnetic north.

^bDegrees from vertical.

not interpreted in further detail here. An additional spectral peak recorded in all data sets (including the reference sensor) was identified at ~0.15 Hz, which is at the microseism peak related to ocean-generated seismic waves [Longuet-Higgins, 1950].

Phase relations were explored from simultaneous data generated at sensor positions *B* and *C* (Figure 1). E-W horizontal records were found to be in phase at *f*₁ and out of phase at *f*₂, while vertical records were found to be in phase at *f*₃ and out of phase at *f*₄. These results provide experimental insight into the vibrational mode shapes, suggesting that *f*₁ represents the first horizontal bending mode (shape akin to a half sine wave), *f*₂ represents the second horizontal bending mode (shape akin to a full sine wave), while *f*₃ and *f*₄ are the first and second vertical bending modes, respectively (compare to mode shapes shown in Figure 3).

4.2. Numerical

Numerical modal analysis explored the anticipated mode shapes at *f*₁ through *f*₄. We used the finite-element software Comsol Multiphysics for Eigenfrequency analysis; input data included geometry, boundary conditions, and material properties. We measured the geometry of Mesa Arch in the field using a laser rangefinder combined with tape measurements where possible. The resulting 3-D model was simple but captured the overall distribution of mass within the arch. Boundary conditions were based on field assessment; on the southern end the arch was attached to the cliff at the bottom and a small portion of the back side (Figure 1c), while the northern abutment terminated into intact rock and was held fixed at the bottom and northern sides. For material properties, we assumed a uniform density (ρ) for Navajo sandstone of 2000 kg/m³ [Schultz *et al.*, 2010] and then varied Young's modulus (*E*) to achieve the best fit with measured resonant frequencies. *E* = 5.5 GPa was found to provide optimum match to measured values of *f*₁–*f*₄, which is within the range of expected values for a weathered sandstone rock mass [Hoek and Diederichs, 2006].

Predicted resonant frequencies for Mesa Arch are 3.0, 6.0, 7.1, and 8.1 Hz (Table 1). Despite minor variations between predicted and measured values, our simplified, uniform numerical model was able to closely reproduce the first four resonant frequencies of the arch. Refinements could include a more sophisticated geometrical model, as well as inclusion of material compartments or discontinuities.

Table 2. Repeat Resonant Frequency Measurements From Mesa Arch^a

Date (UTC)	Start Time	Duration (hh:mm)	<i>f</i> ₁ (Hz)	<i>f</i> ₂ (Hz)	<i>f</i> ₃ (Hz)	<i>f</i> ₄ (Hz)	Mean Rock Temperature (°C)	Sensor Positions
28/9/2013	02:43	04:21	2.879 ± 0.047	6.017 ± 0.134	6.921 ± 0.126	8.357 ± 0.453	6.5	A, R
13/12/2013	23:30	01:00	3.049 ± 0.132	6.554 ± 0.435	7.568 ± 0.234	-	-7.7	A, R
20/2/2014	20:36	00:54	2.879 ± 0.076	5.878 ± 0.184	6.885 ± 0.170	8.168 ± 0.233	7.8	A, R
12/4/2014	01:20	00:42	3.134 ± 0.516	6.077 ± 0.191	7.211 ± 0.168	8.575 ± 0.371	18.4	A, C
05/5/2014 ^b	18:03	61:26	3.022 ± 0.121	6.121 ± 0.130	7.193 ± 0.226	8.647 ± 0.250	17.0	A, R
16/6/2014	22:42	01:33	3.095 ± 0.039	6.212 ± 0.098	7.378 ± 0.105	8.804 ± 0.147	27.4	A, R
20/8/2014	03:50	01:10	2.925 ± 0.043	6.000 ± 0.104	6.983 ± 0.120	8.372 ± 0.282	16.0	A, -
28/10/2014	19:30	02:00	2.921 ± 0.115	6.084 ± 0.145	7.022 ± 0.135	8.500 ± 0.330	25.3	B, C
06/5/2015	17:45	01:00	2.886 ± 0.040	5.943 ± 0.089	6.895 ± 0.101	8.350 ± 0.127	18.0	D, R

^aError bounds represent 95% confidence limits. Sensor positions A–D shown in Figure 1c; R = reference.

^bAveraged over the 3 day experiment.

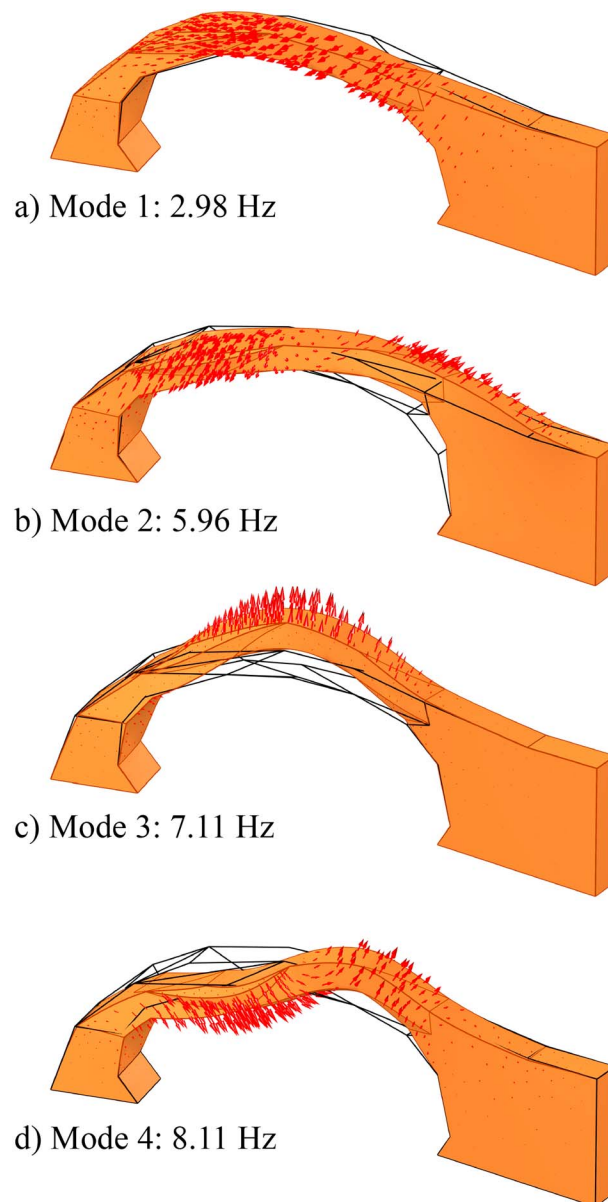


Figure 3. (a–d) Modeled mode shapes and frequencies for the first four resonant modes of Mesa Arch. Arrows and deformed body show displacement at zero phase and are scaled by magnitude; wireframe is the original static form. Animations are shown in Movie S1.

and decreased at night, with overall peak-to-peak daily change of a few percent: f_1 and f_3 varied by $\sim 3\%$, while f_2 and f_4 changed by $\sim 1.5\%$. These variations were directly in phase with rock surface temperature; i.e., resonant frequencies increased with rock temperature with no observable phase offset. Frequency shifts were also correlated with tilt—each day as the arch warmed, thermoelastic expansion caused northward relative tilt at our sensor position, while at night as the arch cooled, tilt increased to the south. In addition to daily trends, we observed a gradual multiday decrease in frequency, tilt, and temperature (Figure 4).

We attribute measured resonant frequency shifts to thermal stiffening of the rock mass. As the rock warmed each morning, thermal stresses increased horizontal compression parallel to the arch (generating measured tilt). Compression likely resulted in increased grain contact stresses and closure of cracks [Zangerl *et al.*, 2008;

Simulated vibrational mode shapes are shown in Figure 3 and Movie S1. The fundamental mode of vibration (mode 1) is out-of-plane horizontal bending (plane of the arch defined as vertical and parallel to the span), mode 2 is the second horizontal out-of-plane bending, mode 3 is the first in-plane (vertical) bending, and mode 4 is the second in-plane bending. These results were confirmed by field assessment of phase relations for sensors located at positions *B* and *C*; see section 4.1. Model results were also used to predict polarization orientations for f_1 – f_4 at a position close to sensor location *A* (Table 1). Our modeled mode 1 is oriented at $102^\circ/89^\circ$ (azimuth/incidence angle), mode 2 is oriented $106^\circ/90^\circ$, mode 3 is oriented $034^\circ/59^\circ$, and mode 4 is oriented $238^\circ/80^\circ$. These results match well with measured data for three out of four modes (Table 1). Only mode 3 differs from our measurements, which may represent a limitation of our simplified model geometry. Polarization data from sensor positions *B*–*D* compared well with model predictions (Figure S3).

5. Resonant Frequency Monitoring

We monitored resonant frequency, tilt, rock and air temperature, and relative humidity at Mesa Arch over a period of 3 days in May 2014. Our experiment began at 12:00 local time on 5 May and ended at 01:30 on 8 May, comprising 61.5 h. During this time, we observed measurable variation in all four of the identified resonant frequencies of Mesa Arch (Figures 4 and S4). Frequencies increased during the day

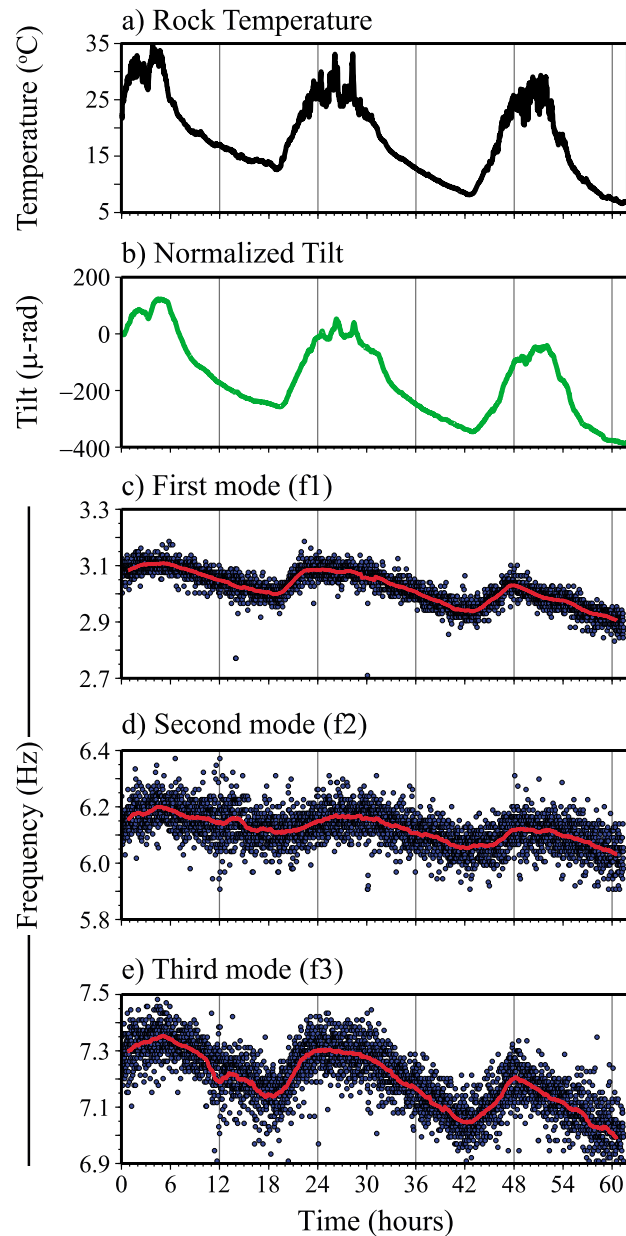


Figure 4. Continuous data from Mesa Arch during the 3 day experiment: (a) rock temperature, (b) relative northward tilt, and (c–e) frequency variation at f_1 – f_3 ; dots are interpolated every minute, and bold trace is smoothed fit. Experiment began at 12:00 local time on 5 May 2014.

with the lack of measured phase shift indicates that the mechanism controlling thermal stiffening occurs within a relatively shallow, surficial region of Mesa Arch.

Repeat measurements of resonant frequencies over ~1.5 years revealed slight changes (Table 2) but without systematic seasonal variation. Comparing frequency shifts with rock surface temperature, we find direct correlation for positive temperatures (Figure S5), confirming that shallow thermal stresses influence resonant frequency shifts. Near-surface rock temperatures vary with the season, time of day, cloud cover, etc. Direct correlation between rock surface temperature and resonant frequencies breaks down, however, at negative temperatures, and frequencies sharply increase. We propose that interstitial ice generated from refrozen snowmelt may cause the bulk elastic modulus of the rock mass and associated resonant frequencies to increase [cf. Bottelin et al., 2013b]. From equation (1) we also note that changes in bulk density through

Gischig et al., 2011], which together caused bulk stiffening of the rock mass and increased the apparent Young's modulus. Measured frequency shifts give indication of the magnitude of this effect as

$$f \propto \sqrt{\frac{E}{\rho}} \quad (1)$$

Assuming constant density, a 3% peak-to-peak change in f indicates a 6% daily change in E . We have no indication that bulk density changed during our experiment, and frequency shifts do not correlate with relative humidity. The proposed stress-stiffening effect overcomes an expected minor reduction in elastic modulus associated with increasing temperature [Xia et al., 2006], as well as changes in geometry and stiffness caused by thermal strain.

Past studies have highlighted the role of thermal stresses in creating structural deformation and resonant frequency shifts. Clinton et al. [2006], studying the resonant frequency of the Caltech Library, observed diurnal fluctuations in the range of a few percent, which they attributed to thermal stiffening. Similarly, Sohn et al. [1999] reported a ~5% daily variation in the fundamental frequency of a concrete bridge, directly correlated with heating of the bridge deck. Meanwhile, Bottelin et al. [2013b] measured daily peak-to-peak variations in resonant frequency of ~4% at a rock column, directly correlated and in phase with temperature. Like Bottelin et al. [2013b], we note that daily temperature changes penetrate to only shallow depths in rock (approximately tens of centimeters), which together

varying saturation should contribute to short-term resonant frequency shifts. However, measurements on 20 August 2014 shortly after an intense rain storm showed no apparent offset from the temperature-frequency trend (Figure S5). In addition, we witnessed several periods of strong winds during our 3 day test at Mesa Arch, and while we have no wind speed data from the time, we found no notable resonant frequency shifts associated with documented windy periods [cf. Lévy *et al.*, 2010]. We did not identify any long-term trends or permanent offsets in resonant frequencies during our study period, which might indicate internal damage.

6. Conclusions

We combined ambient vibration data with 3-D numerical analysis to measure and interpret the resonant frequencies and mode shapes of Mesa Arch in Canyonlands National Park, Utah. In doing so, we have established new methodology to evaluate the response of Mesa Arch to changes in environmental conditions and created a baseline to monitor relative changes in the arch's long-term structural health. We measured daily resonant frequency shifts of up to 3%, correlated with rock temperature and arch deformation, which we propose are generated through thermal stress cycles and associated stiffening and relaxation of the rock mass. Similar scale variations were seen in repeat measurements over >1.5 years but without clear seasonal pattern. Characterizing the magnitude and drivers of these reversible effects is crucial in our ultimate aim of identifying permanent change associated with internal damage. Our study creates new opportunities for geoscientists to draw on the field of structural health monitoring in developing novel means for evaluating damage in natural rock landforms.

Acknowledgments

This study was funded in part by the University of Utah Research Foundation, the National Park Service, and the National Science Foundation grant EAR-1424896 to Moore and Thorne. We thank Jordan Culp and Ben White for their help in the field and Keith Koper for his advice with polarization processing. Comments from two anonymous reviewers are appreciated. We gratefully acknowledge the University of Utah Center for High Performance Computing for computer resources and support. Some figures were created using the Generic Mapping Tools [Wessel and Smith, 1998]. Data generated in this study are available for download at the author's website: <http://geohazards.earth.utah.edu/data.html>.

The Editor thanks two anonymous reviewers for their assistance in evaluating this paper.

References

- Bottelin, P., *et al.* (2013a), Spectral analysis of prone-to-fall rock compartments using ambient vibrations, *J. Environ. Eng. Geophys.*, *18*, 205–217.
- Bottelin, P., C. Levy, L. Baillet, D. Jongmans, and P. Gueguen (2013b), Modal and thermal analysis of Les Arches unstable rock column (Vercors Massif, French Alps), *Geophys. J. Int.*, *194*, 849–858.
- Burjanek, J., G. Stamm, V. Poggi, J. R. Moore, and D. Fäh (2010), Ambient vibration analysis of an unstable mountain slope, *Geophys. J. Int.*, *180*, 820–828.
- Burjanek, J., J. R. Moore, F. X. Yugsi-Molina, and D. Fäh (2012), Instrumental evidence of normal mode rock slope vibration, *Geophys. J. Int.*, *188*, 559–569.
- Carder, D. S. (1936), Observed vibrations of buildings, *Bull. Seismol. Soc. Am.*, *26*(3), 245–277.
- Clinton, J. F., S. Case Bradford, T. H. Heaton, and J. Favela (2006), The observed wander of the natural frequencies in a structure, *Bull. Seismol. Soc. Am.*, *96*(1), 237–257.
- Crawford, R., and H. S. Ward (1964), Determination of the natural periods of buildings, *Bull. Seismol. Soc. Am.*, *54*(6A), 1743–1756.
- Farrar, C. R., S. W. Doebling, and D. A. Nix (2001), Vibration-based structural damage identification, *Philos. Trans. R. Soc. London, Ser. A*, *359*(1778), 131–149.
- Gischig, V. S., J. R. Moore, K. F. Evans, F. Amann, and S. Loew (2011), Thermomechanical forcing of deep rock slope deformation: Part 1. Conceptual study of a simplified slope, *J. Geophys. Res.*, *116*, F04010, doi:10.1029/2011JF002006.
- Hoek, E., and M. S. Diederichs (2006), Empirical estimation of rock mass modulus, *Int. J. Rock Mech. Min. Sci.*, *43*(2), 203–215.
- Koper, K. D., and V. L. Hawley (2010), Frequency dependent polarization analysis of ambient seismic noise recorded at a broadband seismometer in the central United States, *Earthquake Sci.*, *23*, 439–447, doi:10.1007/s11589-010-0743-5.
- Lévy, C., L. Baillet, D. Jongmans, P. Mourot, and D. Hantz (2010), Dynamic response of the Chamousset rock column (Western Alps, France), *J. Geophys. Res.*, *115*, F04043, doi:10.1029/2009JF001606.
- Longuet-Higgins, M. S. (1950), A theory of the origin of microseisms, *Philos. Trans. R. Soc. London A*, *243*, 1–35.
- McNamara, D. E., and R. P. Buland (2004), Ambient noise levels in the continental United States, *Bull. Seismol. Soc. Am.*, *94*(4), 1517–1527.
- Moore, J. R., V. Gischig, J. Burjanek, S. Loew, and D. Fäh (2011), Site effects in unstable rock slopes: Dynamic behavior of the Randa instability (Switzerland), *Bull. Seismol. Soc. Am.*, *101*(6), 3110–3116.
- Park, J., F. L. Vernon, and C. R. Lindberg (1987), Frequency dependent polarization analysis of high-frequency seismograms, *J. Geophys. Res.*, *92*(12), 12,644–12,674.
- Schultz, R. A., C. H. Okubo, and H. Fossen (2010), Porosity and grain size controls on compaction band formation in Jurassic Navajo Sandstone, *Geophys. Res. Lett.*, *37*, L22306, doi:10.1029/2010GL044909.
- Sohn, H., M. Dzwonczyk, E. G. Straser, A. S. Kiremidjian, K. H. Law, and T. Meng (1999), An experimental study of temperature effect on modal parameters of the Alamosa Canyon Bridge, *Earthquake Eng. Struct. Dyn.*, *28*(8), 879–897.
- Sufri, O., K. D. Koper, R. Burlacu, and B. de Foy (2014), Microseisms from superstorm Sandy, *Earth Planet. Sci. Lett.*, *402*, 324–336.
- Wessel, P., and W. H. F. Smith (1998), New, improved version of generic mapping tools released, *Eos Trans. AGU*, *79*(47), 579, doi:10.1029/98EO00426.
- Xia, Y., H. Hao, G. Zanardo, and A. Deeks (2006), Long term vibration monitoring of an RC slab: Temperature and humidity effect, *Eng. Struct.*, *28*(3), 441–452.
- Zangerl, C., K. F. Evans, E. Eberhardt, and S. Loew (2008), Normal stiffness of fractures in granitic rock: A compilation of laboratory and in-situ experiments, *Int. J. Rock Mech. Min. Sci.*, *8*, 1500–1507.